**AIAA-2000-4219**

# NAVIER-STOKES ANALYSIS OF A HIGH WING TRANSPORT HIGH-LIFT CONFIGURATION WITH EXTERNALLY BLOWN FLAPS

Jeffrey P. Slotnick*, Michael Y. An, Stephen J. Mysko, and David T. Yeh
*The Boeing Company-Long Beach*

Stuart E. Rogers and Karlin Roth*
*NASA Ames Research Center*

M. David Baker and Steven M. Nash
*MCAT, Inc.*

## Abstract

Insights and lessons learned from the aerodynamic analysis of a High Wing Transport high-lift configuration are presented. Three-dimensional Navier-Stokes computational fluid dynamics simulations using the OVERFLOW flow solver are compared with high Reynolds-number test data obtained in the NASA Ames 12-Foot Pressure Wind Tunnel facility. Computational analysis of the baseline High Wing Transport high-lift configuration with and without externally blown flap jet effects is presented. Using the developed computational fluid dynamics analysis capability, several aerodynamic investigations, including an assessment of nacelle strake effectiveness and wake vortex prediction, are presented.

## Introduction

To reduce the costs associated with the design, development, and manufacturing of modern transport aircraft, major improvements in both aircraft development cycle (time-to-market) and affordability (flyaway cost) must be achieved in order to make new concepts commercially viable. An important driver in reducing aircraft development cycle time and total system cost is the reduction of aerodynamic design cycle time.

To enable these improvements, significant efforts to utilize computational fluid dynamics (CFD) for high-lift system design are underway. Effective use of CFD could greatly reduce the amount of wind tunnel testing required in the design process, and thereby reduce development cycle time and cost. Emerging Navier-Stokes methods have the ability to model the viscous-dominated flow physics associated with advanced transport aircraft aerodynamics. However, to be successful, CFD methods must be easy to use, fast, and *accurate*.[1]

High-lift analysis is particularly challenging, and is a pacing item in reducing aerodynamic cycle time. Computational analysis of realistic high-lift systems is currently limited by configuration geometric complexity, and the wide range of flow phenomena typically present in high-lift flow-fields. High-lift aerodynamics is extremely complex, and is dominated by viscous flow phenomena, such as separation, shock-boundary layer interactions, and multiple element merging confluent wakes.[2] A significant body of work has been performed in two dimensions (2D) to characterize high-lift flow physics.[3-6] An excellent summary of 2D high-lift CFD is given by Ying.[7] Although 2D Navier-Stokes analysis is beginning to make inroads into the high-lift system design process, high-lift flows are inherently three-dimensional (3D). Testing and simulation of complete transport configurations are required to accurately predict high lift system performance.

In recent years, much progress has been shown in the ability to simulate 3D high-lift flow-fields using Navier-Stokes methods. Building block CFD computations on wings with full-span and part-span flaps,[8-10] and on more complicated wing/body geometries[11] have illustrated the range of applicability of present tools, and highlighted the shortcomings still present in Navier-Stokes methods. However, computing the three-dimensional subsonic flow over a complete transport high-lift configuration remains as one of the most difficult challenges of modern CFD.[12,13] Moreover, the simulation of powered, high-lift systems, such as the inclusion of engine jet impingement effects on an externally blown flap (EBF), has not been explored.

* Senior Member, AIAA.

Under the Integrated Wing Design (IWD) element of the NASA Advanced Subsonic Technology (AST) program, significant effort was concentrated on developing advanced design methodologies to enable both the reduction of design cycle time, and the development of advanced aerodynamic concepts. Within the AST-IWD high-lift subelement, high Reynolds number test data was obtained and used to gain insight into high-lift flow physics, and to calibrate high-fidelity Navier-Stokes numerical simulations. As part of this activity, advanced computational tools were developed to enable production level CFD analysis of three-dimensional high-lift systems on complete transport configurations.[14] As a result of these efforts, the analysis time associated with generating a CFD simulation from geometry to final solution on a complete high-lift transport configuration was reduced by an order of magnitude. This technology was extensively used in the current work to computationally analyze the aerodynamic performance of a High Wing Transport (HWT) high-lift configuration with EBF jet effects.

The AST-IWD program designed, built, and tested an experimental semi-span model of an HWT aircraft in high-lift mode. The main objectives of the HWT wind-tunnel test program included the development of semi-span, powered testing methods, and the evaluation of advanced flap concepts. Perhaps the most important goal, and the focus of the current work, was to provide quality data for CFD code calibration .

This paper gives an overview of the numerical simulation of the complete 3D HWT landing configuration using Reynolds-Averaged Navier-Stokes (RANS) methods. Rather than concentrating on the numerical details of the CFD simulations themselves, an assessment of the predictive capability of the computational method relative to test data is emphasized. Several technical issues, including test facility wall interference effects and jet modeling effects, are presented and discussed in detail. The application of the computational method to study nacelle strake effectiveness and wake vortex prediction is also highlighted.

## HWT Configuration

Both the experimental and computational models consist of a fuselage, a wing with high-lift system, a winglet, and two under-wing-mounted nacelles at 30% and 56% span, respectively. The high-lift system is composed of three slat segments on the wing leading-edge, and a double-slotted (vane/flap) flap aft of the main wing. The flap is attached to the main wing with four hinged brackets, which are covered by fairings. Inboard and outboard nacelle strakes are located on each of the nacelles. Neither the experimental nor the computational model included an empennage.

## Experimental Data

Under the AST-IWD program, extensive high Reynolds number powered test data was obtained for the semi-span HWT model in the NASA Ames Research Center 12-Foot Pressure Wind Tunnel (PWT) facility. Turbine Powered Simulator (TPS) units were used to simulate the engine exhaust flow. Data collected included standard force and moments, and a vast array of surface pressure transducer measurements on the fuselage, the main wing, the high-lift elements (slat, vane, and flap), and winglet. Also, flow-field pressure and temperature measurements were obtained using the Boeing Quantitative Wake Survey System (QWSS).[15] An additional test entry, designed for TPS calibration, was used to collect jet flow-field data using QWSS for a single TPS unit mounted on a sting support.

All experimental data and computational results are subject to the Limited Exclusive Rights provisions of the NASA AST contract, and are considered sensitive. Because of this, all axis labels have been removed from the data plots.

## Computational Analysis

**Grid Generation.** The Chimera overset grid method was employed to discretize the HWT surface and volume domain.[16] The Chimera Grid Tools package[17], coupled with an advanced grid scripting system,[11,14] was used to generate the majority of the grid system. A complete summary of the grid generation tools and processes used to build the HWT high-lift configuration grid system is reported by Rogers et al.[18] For the work presented here, the computational model of the HWT high-lift landing configuration installed in a computational model of the NASA Ames 12-Foot PWT facility is shown in Fig. 1.

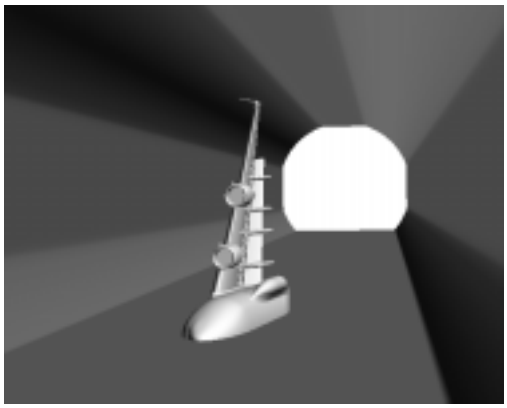

Figure 1. HWT computational model geometry.

The computational geometry of the wind tunnel includes an inviscid, simplified model of the test section, and neglects the effects of viscosity of the test section splitter plate and semi-span mounting apparatus, as well as the divergence of the wind tunnel walls downstream of the test section. The simplified inviscid-tunnel model has been shown to be as accurate at simulating wind-tunnel wall interference as the complete viscous-tunnel approach. [19] The HWT overset grid system is composed of 153 grids and 35.2 million grid points, and contains all of the geometry components on the experimental model, except the slat and vane brackets. Fig. 2 shows the HWT high-lift surface grid system, with only every other point in each direction shown. Grid topologies and densities for the high-lift system components are based on results from earlier 2D studies.[3] Box grids were used to discretize the volume to the far-field boundaries. Inter-grid communication was established using the PEGSUS code.[20]

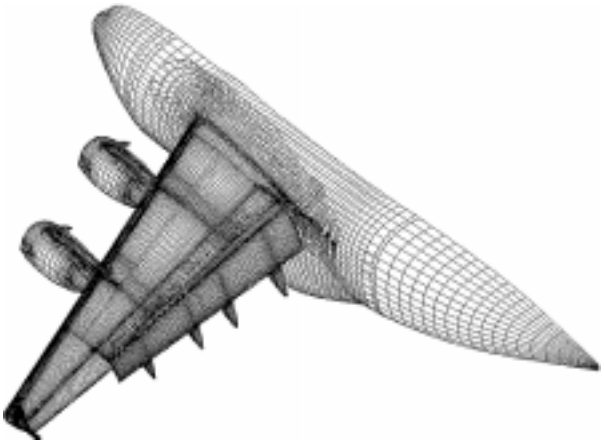

Figure 2. HWT surface grid system.

**Flow Solver.** The OVERFLOW finite-difference Navier-Stokes flow solver,[21] with multigrid convergence acceleration,[22] was used to solve the viscous HWT high-lift flow-field. The ARC3D diagonal scheme was used on the left-hand side of the flow equations. Third-order Roe upwind differencing was used for the right-hand side. Thin-layer viscous terms in all three directions were used in all grids. Low Mach number preconditioning was used in all box grids. Component forces and moments are computed within OVERFLOW using "zipper" grid information supplied by the FOMOCO[23] utility MIXSUR.

**Turbulence and Transition Modeling.** Based on results from previous 2D high-lift studies,[3-6] the Spalart-Allmaras (S-A) one-equation turbulence model[24] is currently accepted as the most appropriate turbulence model for multi-element high-lift flow-field analysis. In conjunction with upwind differencing used in the HWT flow-field simulations, the S-A model demonstrates good overall convergence and robustness. However, as will be discussed later, the use of the S-A model is not successful in predicting the spreading and mixing of the EBF jet flow.

A significant body of research in boundary-layer transition and relaminarization for high-lift flow-fields exists in the literature.[6,7,25] Although it is concluded that modeling transition is critical in predicting the velocity deficits in the confluent wakes accurately for 2D multi-element airfoils, the ability to model transition for complete 3D configurations currently does not exist. For this reason, coupled with a lack of adequate HWT transition location data, all computations are performed assuming fully turbulent flow everywhere.

**Solution Details.** All HWT high-lift configuration OVERFLOW simulations were performed on either a 16 processor Cray C90 or a 128 node Silicon Graphics (SGI) ORIGIN 2000 (O2K) computing platform. A new, multi-level parallel version of OVERFLOW, known as OVERMLP,[26] was used on the O2K. A total of 47 different HWT cases have been computed for different geometry configurations and flow conditions within the AST program. Each of these cases required between 200 to 400 Cray C90 CPU hours, or 1000 to 2000 O2K CPU hours, depending on the angle-of-attack and the power setting. For most cases, convergence to a steady-state was achieved with approximately 2000 multi-grid cycles. These cases were considered converged when the change in total configuration lift coefficient over the last 100 cycles was less than 0.001. A detailed summary of typical OVERFLOW convergence characteristics for large-scale transport high-lift configurations is reported by Cao et al.[12]

## Results and Comparisons

**Baseline Configuration**. Both experimental data and computational simulations for several HWT configurations at various flow conditions and flap deflections were obtained during the AST/IWD program. In this paper, the baseline configuration modeled with CFD is defined as the nominal landing HWT high-lift geometry with slats and a single double-slotted (vane/flap) flap deflected. To evaluate the capability of the OVERFLOW code to accurately predict the aerodynamic performance of the baseline HWT high-lift configuration, several simulations with and without EBF power effects at a range of angle-of-attack were computed. The freestream Mach number ($M_\infty$) was 0.175, and the Reynolds number based on mean aerodynamic chord (MAC) was 13 million.

In Fig. 3, total configuration lift coefficient versus angle of attack is plotted. In Fig 3a, test data not corrected for wall interference (uncorrected) is compared with CFD simulations with wind tunnel walls modeled in both unpowered ($c_\mu$=0.03) and powered ($c_\mu$=0.5) modes, where $c_\mu$ is the engine thrust coefficient. Fig 3b shows corrected test data compared with free-air CFD results. For illustration purposes, the linear portions of each experimental lift curve in Fig. 3a have been extrapolated and are plotted with black, dashed lines. Numbers are used to denote CFD datapoints at specific angles-of-attack. Wall interference corrections to the experimental data have been determined using the Two Variable Method,[27] which is based on surface pressure integration using interpolated and extrapolated wall-pressure measurements.

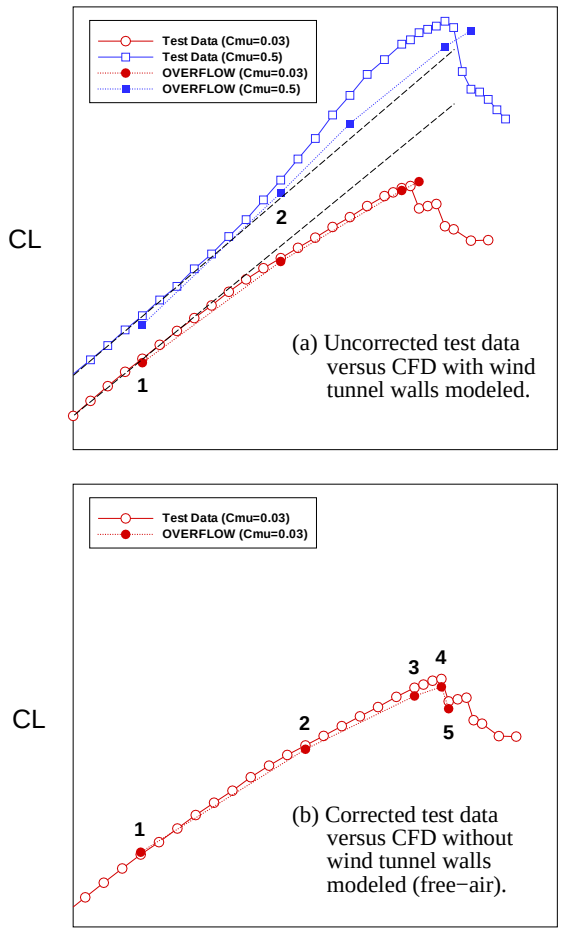


Figure 3. Comparisons of total configuration lift.

In general, the unpowered CFD results, with and without wind tunnel walls modeled, compare very well with respective test data up to maximum lift. For the free-air OVERFLOW simulations, an additional solution beyond maximum lift was obtained. Wing surface pressure comparisons for the unpowered cases are also excellent, demonstrating that both the integrated forces and local flow details are captured. Figure 4 shows slat, main wing, vane, and flap pressure comparisons at 42% span between free-air OVERFLOW results and corrected test data at the five angles-of-attack indicated in Fig 3b.

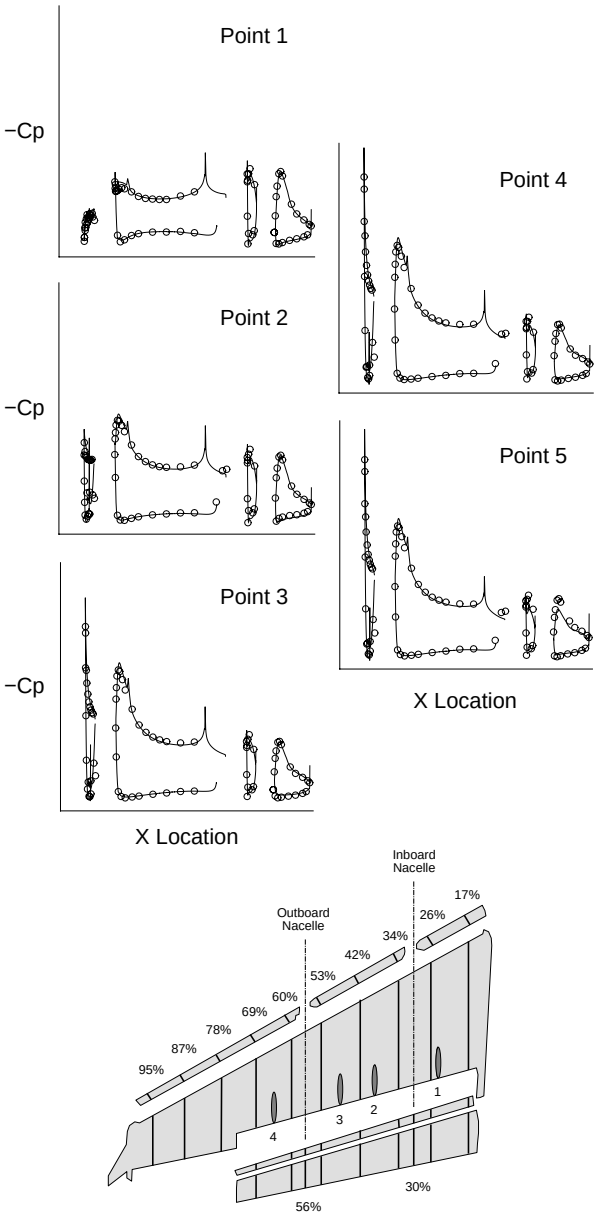


Figure 4. Surface pressure comparisons at 42% span, $c_\mu$=0.03 ( ∘ Corrected test data, — free-air OVERFLOW solutions)

Also shown is the wing pressure transducer layout, with the high-lift elements in exploded view form. A row of pressure transducers was located at 42% span specifically to capture the flow in the region of the

high-lift system where EBF effects are minimal, halfway between the two nacelles.

As can be seen, experimental pressures agree well on all the high-lift elements. The slat, and corresponding wing leading edge, peak pressure increase with increasing angle-of-attack is well captured by CFD. Vane and flap pressures compare well between CFD and test data up to maximum lift. Beyond maximum lift, however, OVERFLOW results show a sharper decrease in lift on the vane and flap elements relative to experimental data. We believe, based on these results, that OVERFLOW does accurately predict the unpowered HWT high-lift flow-field up to maximum lift. However, further studies are required to properly determine if current Navier-Stokes methods can simulate the complex flow breakdown mechanism encountered at stall.

Unlike the unpowered comparisons, the powered computational results differ markedly from the corresponding experimental results. The test data shows a distinct non-linear increase in the lift-curve slope at high, pre-stall angles of attack. Although the exact mechanism is not well understood, it is believed that the non-linearity in the lift-curve slope of the powered test data is principally due to wind-tunnel wall interference effects.

**Wind Tunnel Wall Interference Effects**. To illustrate the relative proximity of the HWT high-lift system with respect to the tunnel test section, Mach number contours on a spanwise cutting plane through the inboard nacelle, pylon, and wing components are shown in Fig. 5.

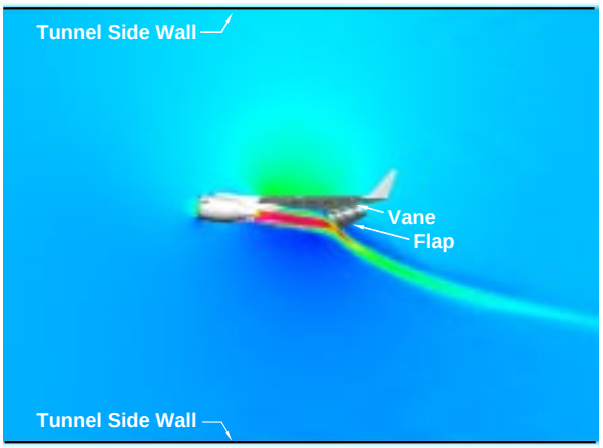


Figure 5. Mach number contours in inboard nacelle/pylon pitch plane.

The outboard nacelle/pylon and flap hinge fairings are not drawn for clarity. The surfaces of the wind tunnel side walls are depicted with heavy black lines. As seen in this tunnel top view, the EBF-deflected jet is forced to bend downstream (upward) prematurely at the wall. Because of this, a reactive force effectively pushes the jet vertically upward. The jet impinges higher on the flap, the flap normal force is increased, and overall wing circulation levels are elevated due to more jet flow through the vane and flap gaps. As a result, the total configuration lift increases.

Unfortunately, no independent test data exists to quantify the wall-interference effects. However, significant insights into wind-tunnel-wall interference have been obtained using CFD, even though the powered OVERFLOW results show only a slight non-linearity in lift-curve slope at the higher angles of attack. In Fig. 6, the slat, main wing, vane, and flap surface pressure comparisons between OVERFLOW solutions with and without wind tunnel walls modeled, at the second alpha point indicated in Fig. 3a, are plotted.

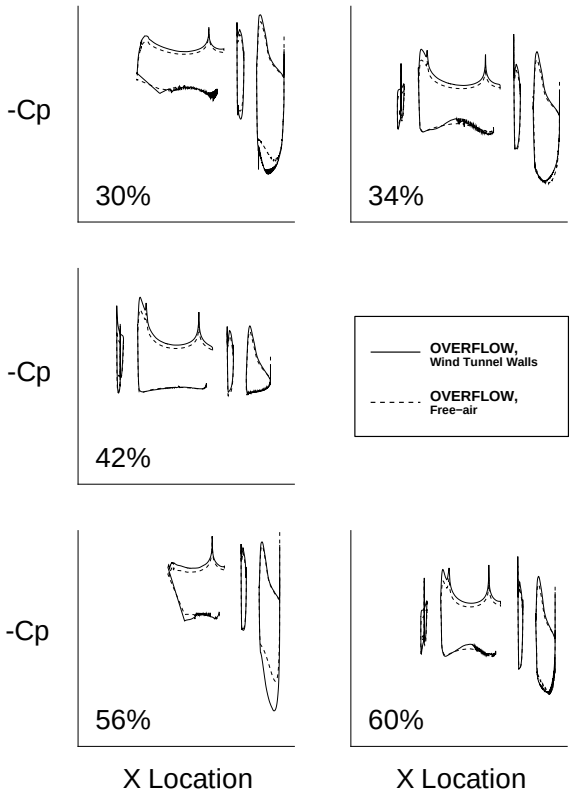


Figure 6. Surface pressure comparisons, $c_\mu$=0.5.

As expected, the presence of the wind tunnel walls provides more suction on the upper-wing surface. However, at 30% and 56% span, the flap lower surface pressures are significantly higher in the computation with walls modeled, relative to the free-air simulation. Moreover, at 30% span (the location of maximum jet

impingement), the peak pressure on the flap occurs further forward towards the flap leading edge in the wind-tunnel wall solution. This is indicative of the jet being pushed vertically upward due to the presence of the walls.

Although the CFD solutions contain a discernible wind-tunnel wall interference effect, there are several other plausible reasons that may account for the differences between CFD and test data. For the complicated HWT model, the use of a simplified wind tunnel computational model, for example, may not adequately represent the true flow in the tunnel. The inclusion of the semi-span splitter plate and related hardware may be required to compute the correct tunnel dynamic pressure. Also, there may be inadequate grid density or resolution in critical regions of the flow-field for the powered simulation. However, the most likely explanation for the discrepancy between CFD and experimental data is inadequate turbulence modeling in the EBF jets.

**Jet Flow Simulation Capability.** Even though deficiencies in the turbulence modeling of the EBF jet flow affect the computational prediction of HWT aerodynamic performance at all angles-of-attack, the shortcoming is clearly illustrated at a relatively low angle-of-attack. Fig. 7 shows the slat, main wing, vane, and flap element surface pressure comparisons between CFD and test data at five spanwise rows of pressure taps for both unpowered (a) and powered (b) simulations, at the first alpha point indicated in Fig. 3a. For the unpowered case, surface pressure comparisons between CFD and experimental data for the baseline HWT configuration show excellent agreement. For the powered case, OVERFLOW fails to predict the large pressure rise due to the jet exhaust impingement on the flap at 34% and 60% span. As a result, the total lift predicted by OVERFLOW is lower than the test data.

To calibrate the TPS thrust levels in the NASA Ames 12 Foot PWT in support of the HWT model experiment, an isolated TPS test was conducted. As part of this test, QWSS flow-field measurements were obtained at three streamwise locations in the jet exhaust to aid in OVERFLOW code calibration activities for HWT EBF jet-flow simulation.

Figure 8a shows the overset computational model of the TPS calibration setup. The sting-mounted model contains 2.6 million points in 32 grids. All simulations were obtained at a Mach number of 0.2, angle of attack of zero degrees., a Reynolds number of 6.2 million, and a fan rotor speed of 53,000 RPM. Fig 8b shows representative Mach contours in the pitch plane predicted using OVERFLOW for the TPS calibration configuration at these flow conditions. Also depicted are the three streamwise plane stations where QWSS flow-field data was collected.

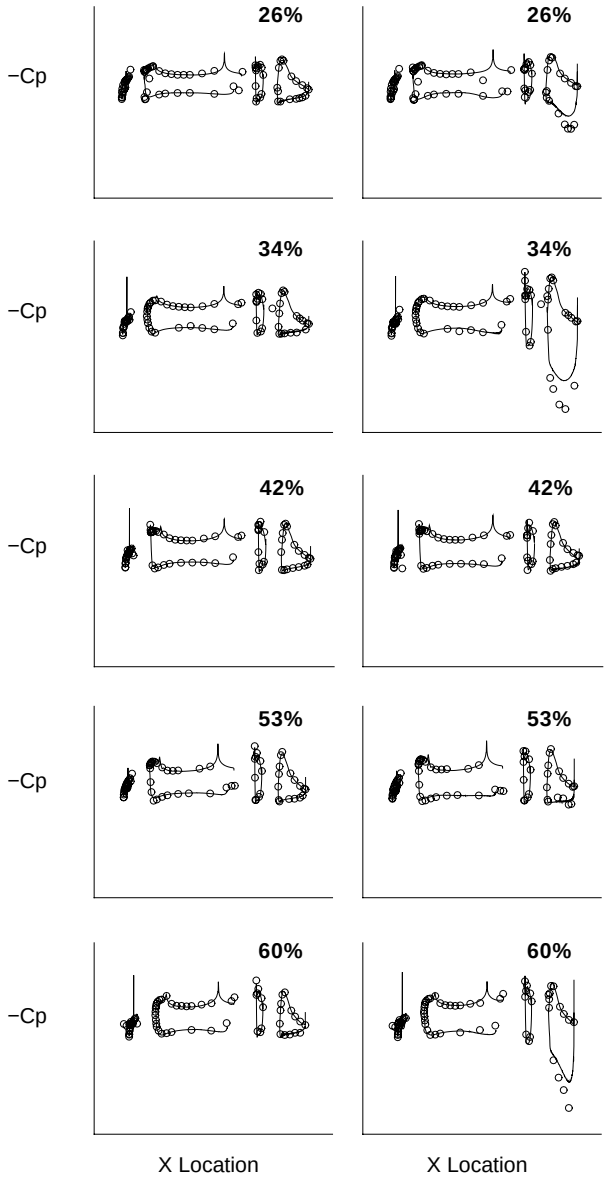


(a) unpowered, cμ=0.03.

(b) power−on, cμ=0.5.

Figure 7. Surface pressure comparisons.
( ∘ Uncorrected test data, — OVERFLOW with tunnel walls modeled)

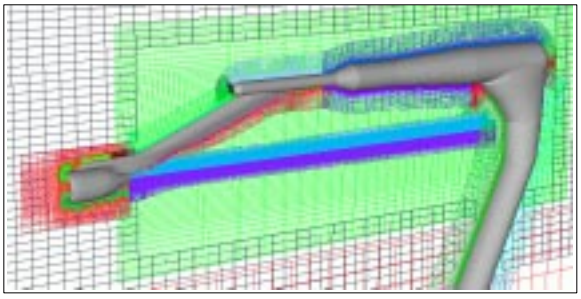

(a) TPS calibration model grid system

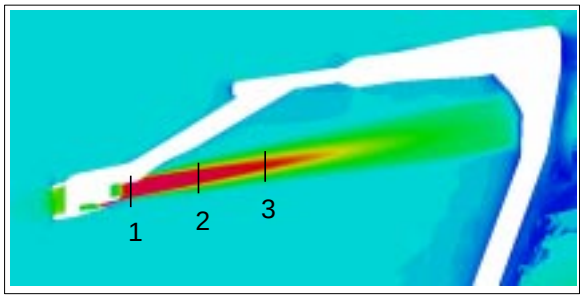


(b) Mach numbers contours, cμ=0.5.

Figure 8. TPS calibration model CFD analysis.

In Fig. 9, Mach contours at these three stations for test data (left) and OVERFLOW using the S-A turbulence model (right) are shown. The fan and core mold line traces are superimposed to better show the comparison of the jet exhaust expansion between the CFD and test data. The experimental data clearly shows an asymmetric distortion of the jet at all three QWSS stations, whereas the computed results were constrained to be symmetric. The experimental asymmetry is likely caused by flow swirl in the TPS unit, and is perhaps influenced by the presence of total-pressure rakes placed asymmetrically inside the fan and core ducts. Also, the test data shows an increasing amount of flow mixing as the jet exhausts downstream. This level of mixing may influenced by the presence of a fine-grain flow straightening mesh placed at the head of the fan duct.

By comparison, the OVERFLOW simulations show markedly lower levels of jet spreading and mixing. Because the CFD results are obtained on a half-model of the TPS calibration geometry without internal duct pressure rakes modeled, no asymmetric distortion is simulated. Also, for the OVERFLOW runs, the engine boundary conditions are set at upstream faces within the fan and core ducts, respectively, based only on average available flow data at these stations. Because of this, the OVERFLOW upstream jet boundary conditions are defined as average, radially-constant flow without swirl. Therefore, there is no mechanism within the numerical simulation to introduce swirl into the solution.

Consider also that the S-A one-equation turbulence model is used in the simulations. Although the S-A model has been shown to be a good general-purpose turbulence model appropriate for high-lift flow analysis, the model was not designed for the prediction of jet flows.[28]

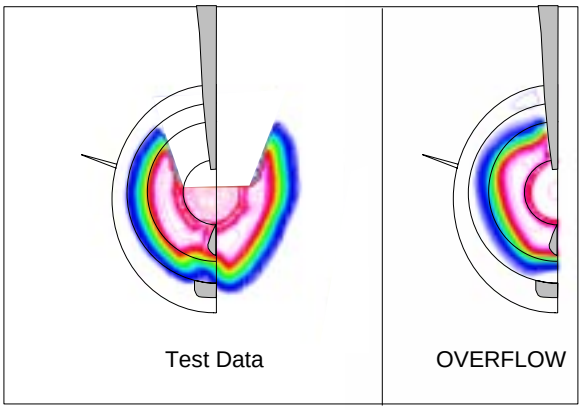


(a) QWSS Plane 1.

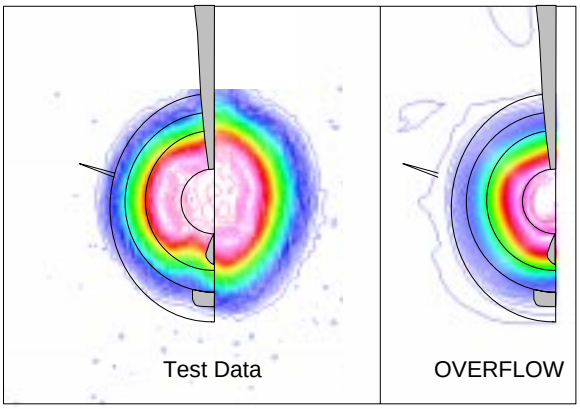


(b) QWSS Plane 2.

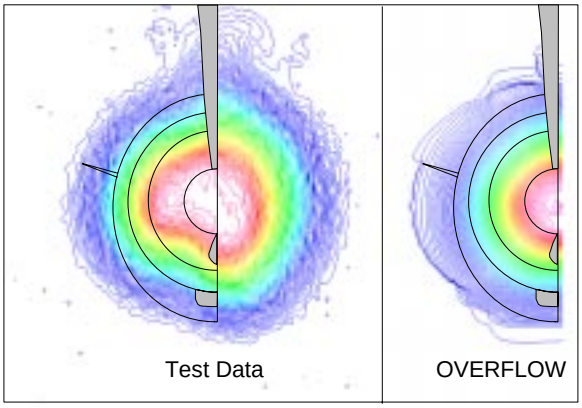


(c) QWSS Plane 3.

Figure 9. QWSS Mach number comparisons.

Based on these results, OVERFLOW does not accurately predict the proper mixing and spreading of the jet-engine exhaust. Specifically, for the complete HWT model, the jet impingement on the flap is confined to a smaller area than in the experiment. This results in lower total-configuration lift relative to the test data. It is clear that without the TPS geometric asymmetries and complex jet inflow flow conditions modeled appropriately in OVERFLOW, exact matching of jet flow features is impossible. However, even with these deficiencies, the matching of gross jet flow magnitudes has been achieved. Further investigation of TPS jet flow-fields with more complex turbulence models is warranted.

## Additional Studies

As demonstrated, complete HWT high-lift computational simulations do not predict exact vehicle performance at either high angle-of-attack conditions and/or high power settings. However, valuable insights into important aerodynamic issues can be gleaned from HWT Navier-Stokes analysis. Two significant issues, nacelle strake effectiveness and wake vortex prediction, were investigated under the AST-IWD high-lift program. A summary of the computational analysis and lessons learned are presented below.

**Nacelle Strake Effectiveness**. Nacelle strakes (or chines) are commonly used to alleviate the adverse aerodynamic affects of wing-mounted high-bypass-ratio engine installations. The close coupling of the large engines with the wing results in increased flow-field interaction at the wing/pylon juncture at high angles-of-attack. Without nacelle strakes, this flow-field interaction results in reduced aircraft performance, especially at maximum lift.[29] Increased understanding of nacelle strake effectiveness is critical to properly optimize strake size and location. If this assessment is to be done numerically, determining the computational requirements to predict nacelle-strake effects is equally as important. For these reasons, the ability of Navier-Stokes CFD methods to capture nacelle-strake effects was evaluated.

OVERFLOW solutions without power ($c_\mu$=0.03) at a moderately high angle-of-attack were obtained for HWT high-lift configurations with all (inboard nacelle and outboard nacelle) strakes on and with all strakes off. As with the previous baseline HWT simulations, the freestream Mach number was 0.175, and the Reynolds number was 13 million based on MAC. Other than the fine grid boxes surrounding the nacelle and main wing structures, no special grid resolution was built into the baseline HWT grid system to specifically capture the nacelle-strake vortices.

Nacelle strakes are designed to increase maximum lift through two flow mechanisms. First, nacelle strakes reduce upwash over the unprotected portion of the main wing near the wing/pylon intersection. As a result, the flow is straightened as it reaches the main wing, thereby relieving some of the adverse effects of the engine installation. Figure 10 shows the surface streamline patterns on the outboard nacelle with strakes off (a) and with strakes on (b). These images clearly show the reduction of flow upwash into the wing/pylon juncture with strakes on. As a result, cross-flow separation on the nacelle near the pylon juncture is reduced (Fig. 11).

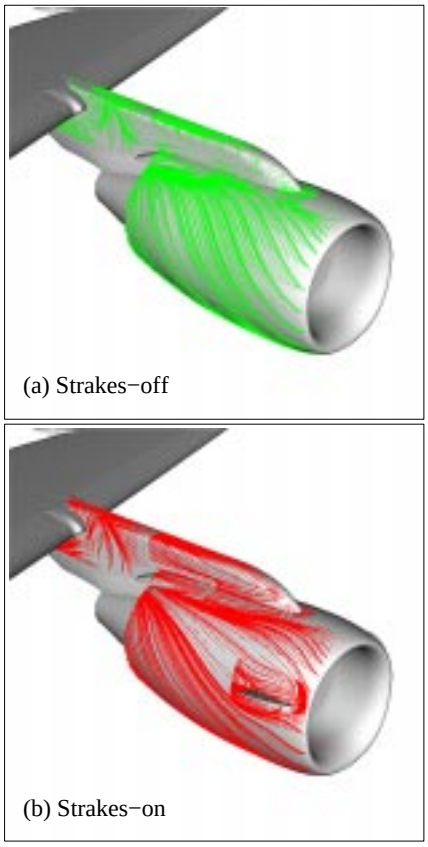


Figure 10. Nacelle surface oilflow.

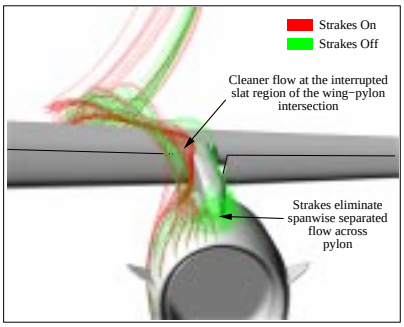


Figure 11. Nacelle strake particle traces.

Second, the presence of the strake vortices provides downwash on the wing upper surface, and serves to energize the boundary layer. Fig. 12 depicts total pressure contours above the wing upper surface at 20% chord aft of the inboard wing/pylon juncture.

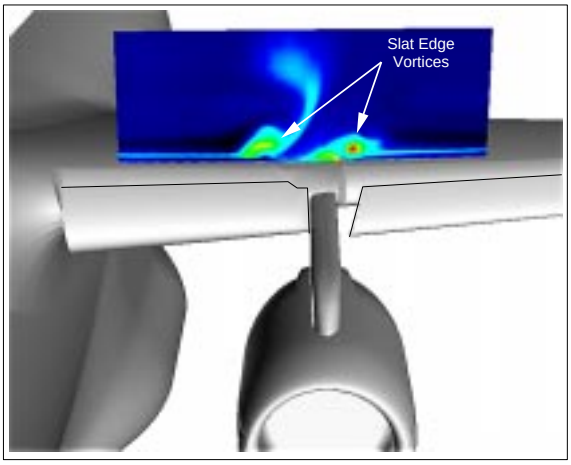


(a) Nacelle strakes off.

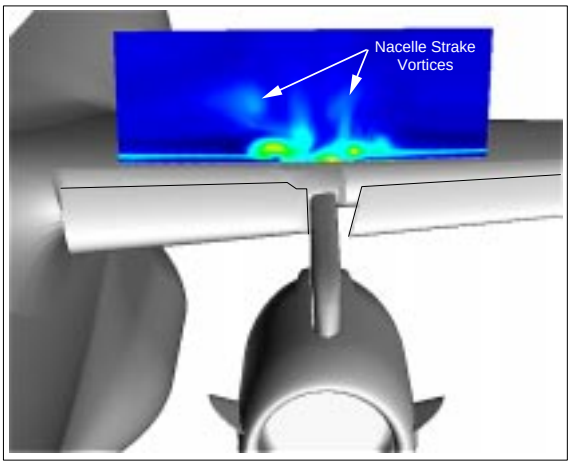


(b) Nacelle strakes on.

Figure 12. Total pressure contours on wing at 20% chord near the inboard nacelle-pylon installation.

For both strake-off and strake-on configurations, the individual slat-edge vortices and slat wakes are well pronounced. For the strake-on case, the nacelle-strake vortices, positioned above the slat-edge vortices, are discernible as well. In the strake-off simulation, as the inboard slat-edge vortex wraps around the upper surface of the wing, it pulls flow away from the surface. In contrast, in the strake-on computation, the strake vortices provide counter-rotating downwash that effectively alleviates this flow behavior. As a result, the health of the boundary layer on the wing upper surface is improved, and flow separation is delayed. Also, note that the presence of the nacelle strakes tends to diminish the strength of the middle-slat-edge vortex.

It is clear that OVERFLOW HWT nacelle strake analysis has yielded valuable insight into the effect of strake vortices on high-lift flow physics. However, use of CFD to predict the actual magnitude of the strake lift increment is not yet appropriate. The strake-lift increment is defined as the difference between total lift with strakes on minus total lift with strakes off. At this moderately high angle-of-attack, experimental data shows a strake-lift increment that is nearly twice the magnitude of that predicted by CFD. The difference in the strake-lift increment can be attributed to two sources. First, the relatively coarse grid used to capture the strake vortices is inadequate to properly simulate the correct amount of vortex dissipation. Second, at this angle-of-attack, the flow is on the verge of separation. The onset of separation near maximum lift is not well predicted by current Navier-Stokes methods. Since nacelle strakes were designed to improve maximum lift, many additional simulations are needed to evaluate the accuracy of Navier-Stokes for flows with incipient separation.

**Wake Vortex Prediction**. Reducing the adverse effects of transport aircraft wake-vortex formation is an important element in increasing airport operation capacity. By reducing wake-vortex turbulence, aircraft separation distances on approach can be decreased. With more aircraft able to serve busy airports, costly delays could be minimized.[30,31]

To alleviate trailing-wake vortices, an understanding of the flow physics associated with wake vortices is important. Moreover, for the baseline EBF-powered HWT configuration, evaluation of the jet-blowing effects on wake vortex formation is critical. Much work on the theoretical understanding of wake vortices exists in the literature,[30] but quantitative evaluation of wake-vortex formation for complete transport configurations using Navier-Stokes methods is not widely available.

During the HWT model test, QWSS flow-field survey data was obtained specifically to study the wake vortex field behind the HWT high-lift configuration. The constant streamwise QWSS measurement plane is located approximately one tip-chord downstream of the wing trailing edge.

To evaluate the capability of the OVERFLOW code to predict the near-field wake vortex structure, several CFD simulations at representative approach power conditions for a variety of flap configurations were obtained, and compared with QWSS data. Figure 13 shows the Mach contour comparison between the QWSS test data (a), OVERFLOW modeled without walls (b), and OVERFLOW modeled with wind tunnel

walls (c), for the baseline landing configuration. The view is looking forward from tail to nose, and valid QWSS data is contained within the concentration of contour lines around the probe sweep perimeter.

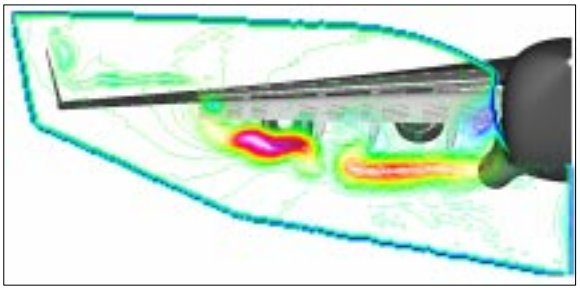

(a) Test data.

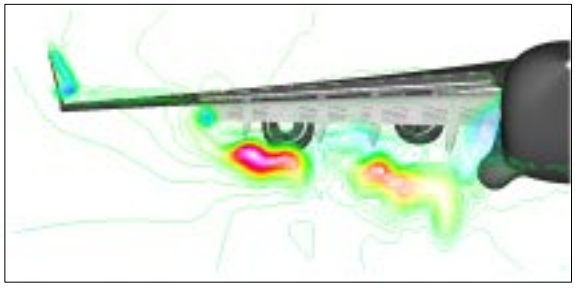

(b) OVERFLOW, free-air.

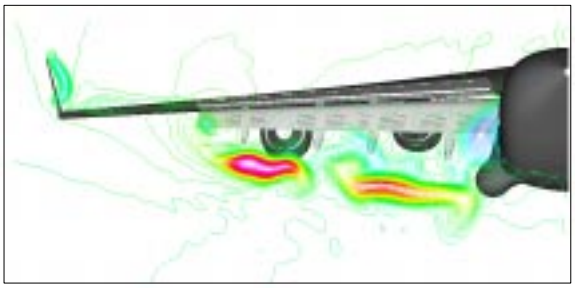

(c) OVERFLOW, wind tunnel walls.

Figure 13. Comparison of Mach number contours in QWSS wake vortex survey plane.

In general, the CFD simulation results modeled with walls and the experimental data agree quite well. The flap edge vortex and winglet-wake are well predicted by OVERFLOW. The distortion of both the inboard and outboard engine jets downstream of the flap is also well simulated by OVERFLOW. The flattened shape of the inboard nacelle jet contour in the QWSS measurement plane gives further evidence of the impact of wind-tunnel wall-interference effects on the wake-vortex flow-field. The free-air CFD result shows some jet exhaust flattening, but not to the same extent as the wind-tunnel wall case. Also, the experimental Mach contours appear to be shifted up vertically relative to both CFD solutions. This indicates that both inboard and outboard jet exhausts are closer to the wing, and further supports the discrepancy in the powered lift-curve slopes between CFD and test data shown earlier.

Fig. 14 shows the vorticity and velocity vector comparison between QWSS-obtained test data and OVERFLOW CFD results. The x-component of vorticity is shown. Red contours indicate clockwise flow, and blue contours indicate counterclockwise flow. The vortex field aft of the wing trailing edge is modeled well using OVERFLOW. The experimental results and CFD simulations both clearly show the strong flap-edge vortex, the winglet junction vortex, and the tip vortex. The vortices in the jet exhaust are washed out due to inadequate grid resolution.

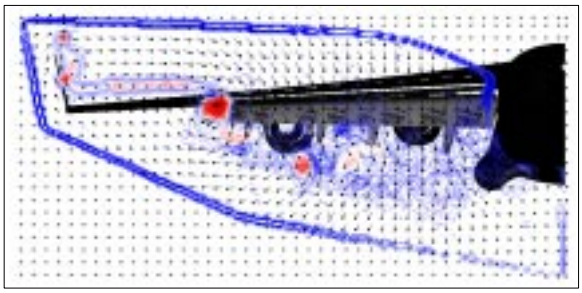

(a) Test data.

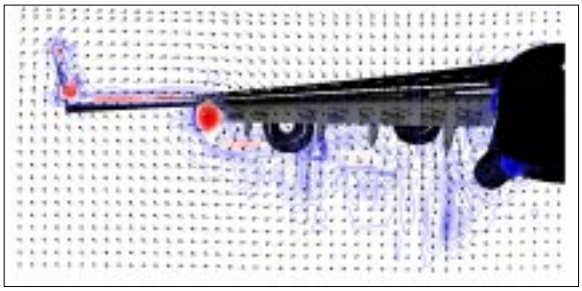

(b) OVERFLOW, free-air.

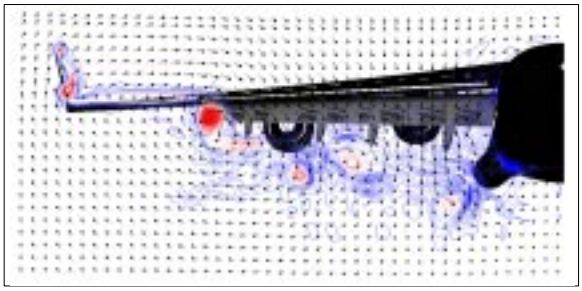

(c) OVERFLOW, wind tunnel walls.

Figure 14. Comparison of vorticity contours and velocity vectors in QWSS wake vortex survey plane.

Close inspection of the differences between CFD and test data show further evidence of the impact of wind-tunnel-wall interference on near-field wake vortex structure. Behind the trailing edge of the flap,

the vortex behind and below the outboard nacelle is well pronounced in the QWSS flow-field survey data. This vortex is shed principally from the flow expanding around flap-hinge fairing #3 (where #4 is the furthest outboard fairing). It is believed that since the jet exhaust is pushed up closer to the wing by the tunnel walls, the spanwise flow is stronger, and thus creates a stronger vortex. The OVERFLOW simulation with wind-tunnel walls predicts a weak vortex, while the free-air CFD solution does not capture the vortex at all.

Based on this initial evaluation, it is believed that OVERFLOW can adequately predict the gross magnitude and location of trailing wake vortices. Grid refinement aft of the main wing will most likely improve the accuracy of these results.

## Conclusions

The OVERFLOW code has been applied to the aerodynamic analysis of the complete HWT high-lift configuration. The comparison of unpowered CFD simulations with experimental data up to maximum lift is excellent. Power-on CFD simulations, however, underpredict the total configuration lift relative to the test data, which exhibits a distinctly non-linear character to the lift curve slope at higher angles-of-attack. Evidence shows that wind-tunnel-wall interference effects is the likely reason for the non-linear lift behavior seen in the test data, while inadequate turbulence modeling for jet flows is one of the likely causes for differences seen between CFD and powered test data.

Although vast improvements have been made to the tools that enable large-scale CFD analysis of high-lift systems, there are still significant shortcomings in the accuracy of Reynolds-Averaged-Navier-Stokes (RANS) methods. Use of current general-purpose turbulence models is not fully applicable for the wide range of flow features (confluent shear layers, vortex-viscous interactions, EBF jet effects, etc.) typically present in high-lift flow-fields. What is needed is an improved turbulence model that is able to adequately simulate the different types of high-lift flow physics present within a given CFD computation. Also, current experience with HWT CFD analysis at the maximum lift condition suggests that RANS methods adequately predict the *location* of flow separation, but fail to predict both the maximum lift magnitude, and the angle-of-attack at stall. Improved technology to accurately predict the onset of separation at critical design conditions is needed.

However, by increasing our understanding of EBF HWT high-lift flow physics, the CFD simulations have been successfully used to gain valuable insights into several aircraft aerodynamic issues. Navier-Stokes analysis has greatly increased our understanding of the flow physics associated with nacelle strakes and their effect on increasing maximum lift. Also, preliminary assessment of OVERFLOW to predict near-field wake vortex characteristics has been successful. As a result, use of OVERFLOW to numerically investigate wake vortex alleviation concepts will be further explored.

Finally, the use of complete-configuration CFD analysis in the advanced stages of a high-lift system design process shows great promise. But, due to the large computational costs associated with the analysis of complex geometries, and current limitations in solution accuracy at critical flow conditions, application of RANS methods for high-lift design is not yet practical.

## Acknowledgments

The authors would like to acknowledge the technical contributions and assistance of M. E. Whitlock and R. C. Potter, The Boeing Company, Pieter Buning, NASA Langley Research Center, and D. C. Jespersen and T. H. Pulliam, NASA Ames Research Center. Also, many thanks to the AST-IWD management team for their valuable leadership and insight: F. T. Lynch, AST/IWD Program and Technical Manager, and D. H. Leopold, High-Lift Task Lead, The Boeing Company, and E. B. Plentovich, AST-IWD Program Manager, and K. M. Jones, High-Lift Subelement Lead, NASA Langley Research Center. This work was funded under the Advanced Subsonic Technology program through NASA contract NAS2-20268.

## References

[1]Lynch, F. T., Potter, R. C., and Spaid, F. W. "Requirements for Effective High Lift CFD," ICAS Proceedings, 20th Congress, Sept. 1996.

[2]Meredith, P. T., "Viscous Phenomena Affecting High-Lift Systems and Suggestions for Future CFD Development," High-Lift System Aerodynamics, AGARD CP-515, Paper No. 19, Sept. 1993.

[3]Rogers. S. E., "Progress in High-Lift Aerodynamic Calculations," Journal of Aircraft, Vol. 31, No. 6, Nov. 1994, pp 1244-1251.

[4]Cao, H. V. and Kusunose, K., "Grid Generation and Navier-Stokes Analysis for Multi-Element Airfoils," AIAA Paper 94-0748, Jan., 1994.

[5]Fejtek, I., "Summary of Code Validation Results for a Multiple Element Airfoil Test Case," AIAA Paper 97-1932, July 1997.

[6]Rumsey, C. L., Gatski, T. B., Ying, S. X., and Bertelrud, A., "Prediction of High-Lift Flows Using

Turbulent Closure Models," AIAA Paper 97-2260, June 1997.

[7]Ying, S. X., "High Lift: Challenges and Directions for CFD," AIAA/NPU AFM Conference Proceedings, China, June 1996.

[8]Baker, M. D., Mathias, D. L., Roth, K., and Cummings, R. M., "Numerical Investigation of Slat and Compressibility Effects for a High-Lift Wing," AIAA Paper 99-0538, Jan. 1999.

[9]Berkman, M. E., Khorrami, M. R., Choudhari, M., and Sadowski, S. S., "Investigation of High-Lift Flow Field of an Energy Efficient Transport Wing," AIAA Paper 99-0926, Jan. 1994.

[10]Mavriplis, D. J., and Pirzadeh, S., "Large-Scale Parallel Unstructured Mesh Computations for 3D High-Lift Analysis," AIAA Paper 99-0537, Jan. 1999.

[11]Nash, S., and Rogers, S. E., "Numerical Study of a Trapezoidal Wing High-Lift Configuration," Paper No. 1999-01-5559, World Aviation Conference, San Francisco, CA., Oct. 1999

[12]Cao, H. V., Su, T. Y., and Rogers, S. E., "Navier-Stokes Analysis of a 747 High Lift Configuration," AIAA Paper 98-2623, July 1998.

[13]Rogers, S. E., Roth, K., Cao, H. V., Slotnick, J. P., Whitlock, M. E., Nash, S. M., and Baker, M. D., "Computation of Viscous Flow For a Boeing 777 Aircraft in Landing Configuration," AIAA Paper 2000-4221, AIAA 18th Applied Aerodynamics Conference, August 2000.

[14]Rogers, S. E., Roth, K., Nash, S. M., Baker, M. D., Slotnick, J. P., Cao, H. V., and Whitlock, M. E., "Advances in Overset CFD Processes Applied to Subsonic High-Lift Aircraft," AIAA Paper 2000-4216, AIAA 18th Applied Aerodynamics Conference, August 2000.

[15]Brune, G. W., "Quantitative Three-Dimensional Low-Speed Wake Surveys," 5th Symposium on Numerical and Physical Aspects of Aerodynamic Flows, Cal State- Long Beach, Jan. 13-15, 1992.

[16]Benek, J. A., Buning, P. G., and Steger, J. L., "A 3-D Chimera Grid Embedding Technique," AIAA Paper 85-1523, July 1985.

[17]Chan, W. M., Nash, S., Buning, P. G., and Rogers, S. E., "Chimera Grid Tools, Version 1.0," NASA Ames Research Center, Moffett Field, CA, June 1999.

[18]Rogers, S. E., Cao, H. V., and Su, T. Y., "Grid Generation for Complex High-Lift Configurations," AIAA Paper 98-3011, 29th AIAA Fluid Dynamics Conference, Albuquerque, NM, June 1998.

[19]Rogers, S. E., Roth, K., and Nash, S. M., "CFD Validation of High-Lift Flows with Significant Wind-Tunnel Effects," AIAA Paper 2000-4218, AIAA 18th Applied Aerodynamics Conference, August 2000.

[20]Suhs, N. E., and Tramel, R. W., "PEGSUS 4.0 User's Manual," AEDC-TR-91-8, AEDC/PA, Arnold Air Force Base, TN, 1991.

[21]Buning, P. G., Jespersen, D. C., Pulliam, T. H., Chan, W. M., Slotnick, J. P., Krist, S. E., Renze, K. J., "OVERFLOW User's Manual, Version 1.8l," NASA Langley Research Center, Hampton VA, 1999.

[22]Jespersen, D. C., Pulliam, T. H., and Buning, P. G., "Recent Enhancements to OVERFLOW," AIAA Paper 97-0644, Jan. 1997.

[23]Chan, W. M., and Buning, P. G., "User's Manual for FOMOCO Utilities – Force and Moment Computation Tools for Overset Grids," NASA TM 110408, July 1996.

[24]Spalart, P. R., and Allmaras, S. R., "A One-Equation Turbulence Model for Aerodynamic Flows," AIAA Paper 92-0439, Jan. 1992.

[25]Dam, C. P., Vijgen, P. M. H. W., Yip, L. P., and Potter, R. C., "Leading-Edge Transition and Relaminarization Phenomena on a Subsonic High-Lift System," AIAA Paper 93-3140, July 1993.

[26]Taft, J. R., "MLP – A Simple Highly Scalable Approach to Parallelism for CFD", NASA HPCCP/CAS Workshop, Aug. 25-27, 1998.

[27]Ashill, P.R., "Boundary-Flow Measurement Methods for Wall Interference Assessment and Correction; Classification and Review," Proceedings, 73rd AGARD Fluid Dynamics Panel Meeting and Symposium on Wall Interference, Support Interference and Flow-field Measurements, Oct. 4-7, 1993.

[28]Bardina, J. E., Huang, P. G., and Coakley, T. J., "Turbulence Modeling Validation, Testing, and Development" NASA TM 110446, Apr. 1997.

[29]Stein, D. E., "Vortex Generators. Case History: Use of Vortex Generators in Aircraft Design," *Airliner*, Oct.-Dec. 1985.

[30]Rossow, V. J., "Lift-generated vortex wakes of subsonic transport aircraft," Progress in Aerospace Sciences, 35 (1999) 507-660..

[31]Wood, W. D., Ed., "Proceedings of the FAA/NASA Workshop on Wake Vortex Alleviation and Avoidance," United States Dept. of Transportation, Cambridge, MS, Nov. 1978.